Hierarchical templating in deposition of semi-covalently imprinted inverse opal polythiophene film for femtomolar determination of human serum albumin

Marcin Dabrowski,[a] Maciej Cieplak,[a,] Piyush Sindhu Sharma,[a] Pawel Borowicz,[a] Krzysztof Noworyta,[a] Wojciech Lisowski,[a] Francis D'Souza,[b,]* Alexander Kuhn,[c,]* and Wlodzimierz Kutner[a,d]**

[a] *Institute of Physical Chemistry, Polish Academy of Sciences, Kasprzaka 44/52, 01-224 Warsaw, Poland*

[b] *Department of Chemistry, University of North Texas, 1155 Union Circle No. 305070, Denton, Texas 76203-5017, United States*

[c] *Univ. Bordeaux, CNRS UMR 5255, Bordeaux INP, ENSCBP, 16 Avenue Pey Berland, 33607 Pessac, France*

[d] *Faculty of Mathematics and Natural Sciences, School of Sciences, Cardinal Stefan Wyszynski University in Warsaw, Woycickiego 1/3, 01-815 Warsaw, Poland*

Abstract

Nanostructured artificial receptor materials with unprecedented hierarchical structure for determination of human serum albumin (HSA) are designed and fabricated. For that purpose a new hierarchical template is prepared. This template allowed for simultaneous structural control of the deposited molecularly imprinted polymer (MIP) film on three length scales. A colloidal crystal templating with optimized electrochemical polymerization of 2,3'-bithiophene enables deposition of an MIP film in the form of an inverse opal. Thickness of the deposited polymer film is precisely controlled with the number of current oscillations during potentiostatic deposition of the imprinted poly(2,3'-bithiophene) film. Prior immobilization of HSA on the colloidal crystal allows formation of molecularly imprinted cavities exclusively on the internal surface of the pores. Furthermore, all binding sites are located on the surface of the imprinted cavities at locations corresponding to positions of functional groups present on the surface of HSA molecules due to of prior derivatization of HSA molecules with appropriate functional monomers. This synergistic strategy results in a material with superior recognition performance.

Integration of the MIP film as a recognition unit with a sensitive extended-gate field-effect transistor (EG-FET) transducer leads to highly selective HSA determination in the femtomolar concentration range.

Keywords

Inverse opals, Protein imprinting, Surface imprinting, Semi-covalent imprinting, Extended-gate field-effect transistor (EG-FET), Human serum albumin (HSA)

Corresponding authors

Maciej Cieplak: mcieplak@ichf.edu.pl,

Wlodzimierz Kutner: wkutner@ichf.edu.pl,

Francis D'Souza: francis.dsouza@unt.edu,

Alexander Kuhn: kuhn@enscbp.fr

Introduction

Inverse opals are highly-organized macroporous materials. They gained a wide interest because of the well-defined regular structure and well-developed surface as well as unique optical properties. Prospective applications of these materials involve improved devices for energy conversion and storage (Li et al. 2012; Reculusa et al. 2011), heterogeneous catalysts (Choi et al. 2016; Collins et al. 2013), filters (Wang et al. 2010), photonic crystals (Diao et al. 2013; Kuo et al. 2007; Zheng et al. 2014) as well as chemo- (Holtz et al. 1998; Szucs et al. 2016; Zhao et al. 2009) and biosensors (Li et al. 2009; Szamocki et al. 2006; Yang et al. 2008). Electrodeposition of a conducting material inside a colloidal crystal is one of the most convenient methods of inverse opal fabrication. It enables very precise control over morphology and thickness of the deposited film by controlling the number of spherical nanoparticle (NP) layers with voids in the colloid crystal filled with the deposited material. Current oscillations during potentiostatic deposition of the film provide the desired control because of a periodical change of active surface area (Heim et al. 2012). That way, inverse opals of metals (platinum, gold, nickel, etc.) and conducting polymers (e.g., polypyrrole) were deposited (Walcarius 2010). Among the latter, polythiophenes are very attractive because of their desirable properties including high chemical stability, ease of derivatization, ease of polymerization, etc. (Huynh et al. 2015). However, polythiophene deposition on a colloidal crystal is challenging because of its tendency to form fragile 'hollow spheres' instead of inverse opals (Bartlett et al. 2001). Nevertheless, macroporous polythiophene could also be deposited in the form of an inverse opal crystal under appropriately selected conditions (Cassagneau and Caruso 2002). However, the deposition procedure was not fully optimized and, importantly, current oscillations during potentiostatic film deposition were not observed. Therefore, optimization of electrochemical fabrication of polythiophene inverse opals may improve fabrication technology of many functional materials, such as recognition units in chemosensors.

Molecularly imprinted polymers (MIPs) are among the most promising molecular recognition materials used for chemosensing. MIPs reveal several uncompromised advantages. However, molecular imprinting of macromolecular compounds, such as proteins, is still challenging because direct extension of imprinting procedures developed for low-molecular-weight compounds is ineffective (Bossi et al. 2007; Erdossy et al. 2016; Li et al. 2014). This is

mainly because the permeability of the polymer network for macromolecules to reach the molecular cavities in the MIP is hindered and, moreover, solubility of proteins in most organic solvents is also very low. These disadvantages can be eliminated by surface imprinting (Dechtrirat et al. 2012). Furthermore, application of colloidal crystals as supports for immobilization of these macromolecular compounds and electrochemical fabrication of inverse opals results in materials with high specific surface area and a precisely controlled 3-D structure (Heim et al. 2012).

Other difficulties encountered with protein imprinting involve their conformational and structural instability in harsh environments, such as aggressive organic solvents, high ionic strength, extreme values of pH or temperature, etc. This instability can lead to formation of deformed and inaccurate molecular cavities unable to accommodate and bind native proteins effectively. Moreover, application of functional monomers is not straightforward because the excess of recognition sites in the MIP, randomly distributed outside the imprinted cavities, promotes nonspecific protein adsorption, which results in low chemosensor selectivity. Semi-covalent imprinting may be considered as one of the strategies for surmounting these deficiencies (Cieplak et al. 2015). This strategy leads to geometrically homogenous and well-defined molecular cavities. However, its application to protein imprinting is not trivial.

Some successful attempts of combining protein surface imprinting with macroporous film deposition have already been reported. Some of them use free-radical polymerization (Hu et al. 2007; Liu et al. 2013; Zhou et al. 2011), which in comparison to electrochemical polymerization is more tedious and does not allow such a precise control of the deposition. In other studies, electrochemical polymerization was used. However, structures obtained were far from those of inverse opals (Li et al. 2013) or resulted merely with one half-layer inverted opals (Bognar et al. 2013). Despite numerous difficulties, which still remain to be solved, nano- and microstructured MIP films gain more and more interest (Bompart et al. 2012; Hu et al. 2008; Lautner et al. 2011; Linares et al. 2009; Zdunek et al. 2013).

In the present work we introduce a new synergistic strategy successfully combining three different approaches, namely semi-covalent and protein surface imprinting, and inverse opal structuring, to prepare a recognition material with a hierarchical structure. This new recognition

material, selective with respect to human serum albumin (HSA), with strictly controlled nanostructure at three different scales was devised, fabricated, and tested. The first level of structuring of the material covers the range of hundreds of nanometers. It is based on inverse opal structuring and provides a high specific surface area of the material. The second level is in the range of few nanometers with molecularly imprinted cavities present exclusively on inner surfaces of the pores. The third level involves orientation of all recognition sites of functional monomers on the surface of the imprinted cavities. This orientation is complementary to the orientation of binding sites of the analyte molecule. To achieve this goal, we prepared a hierarchical template for further structuring of the polymeric material. Toward that end, a colloidal crystal template of SiO_2 NPs was prepared using the Langmuir-Blodgett (LB) technique (Scheme 1 step I). Then, template molecules of HSA, derivatized with bithiophene functional monomers (Cieplak et al. 2015), were immobilized on the surface of these NPs (Scheme 1 step II, III). In the second stage, poly(2,3'-bithophene) film was electrosynthesized and simultaneously deposited in the hierarchical template prepared (Scheme 1 step IV). Removal of the NPs and HSA from the resulting MIP led to a polymeric inverse opal material with molecular cavities present exclusively on the inner side of the pore wall (Scheme 1 step V). Moreover, all binding moieties of the functional monomers were present only on the surface of the imprinted cavities. At each stage of MIP preparation, the samples were imaged with scanning electron microscopy (SEM), in order to verify the 3-D structure.

[Here Scheme 1]

Experimental Section

Fabrication of inverse opals surface imprinted with HSA. For preparation of a colloidal crystal of silica NPs, Langmuir films of these NPs were prepared, and subsequently transferred using Langmuir-Blodgett (LB) onto an Au coated glass slide. For that, first, the NPs with their surface modified with 3-aminopropyltriethoxysilane were washed, as described previously (Reculusa et al. 2004; Reculusa and Ravaine 2003, 2005). Next, purified and dehydrated NPs were suspended in a mixed solvent solution of anhydrous ethanol and chloroform (1 : 4, *v* : *v*) at the NP concentration of ~10 mg/mL. Then, the resulting suspension was evenly spread over the air-water interface of the Langmuir trough filled with the Milli-Q water. After organic solvent

evaporation, the NPs floating at the air-water interface were compressed with a barrier speed of 10 cm^2/min to the target LB transfer pressure of 6.0 mN/m (Duffel et al. 2001). Then, the Au coated glass slides were rinsed with water, then methanol, and then acetone. Subsequently, they were cleaned with 50 W oxygen plasma under oxygen pressure of 0.25 kPa for 10 min. Freshly plasma cleaned Au coated glass slides were used as substrates for LB deposition of the colloidal NP crystals. For this deposition, the substrate was immersed, and then withdrawn from the subphase four times, at the speed of 38 mm/min (the maximum speed available) and 1 mm/min, respectively. After the first withdrawal, the deposited crystal was dried and heated to promote adhesion of the NPs of the innermost layer to the Au electrode surface.

To immobilize HSA on the colloidal crystal, the Au film coated glass slides with deposited colloidal crystals were immersed in 2.5% glutaraldehyde for 1 h at room temperature. After washing with Milli-Q water 3 times, the crystals were immersed in a PBS (pH = 7.4) solution of 3 mg/mL bithiophene derivatized HSA overnight at 4 °C. Finally, the crystals were rinsed with PBS buffer, and then 3 times washed with Milli-Q water.

Synthesis and deposition of an MIP film on the surface of an Au-glass slide were simultaneously performed by potentiostatic polymerization at 1.30 V vs. Ag|AgCl pseudo-reference electrode. Both, bare and the colloidal crystal coated Au glass slides were used for this deposition. A propylene carbonate solution of 0.5 M 2,3'-bithiophene (the cross-linking monomer), and 3.0 M $LiClO_4$ (the supporting electrolyte) was used for preparation of MIP and NIP films by electropolymerization. After electropolymerization, the MIP films were rinsed with methanol to remove non reacted monomers and the electrolyte, and then dried in air. A non-imprinted polymer (NIP) control film was deposited on the template-free colloidal crystal using the same solution and electropolymerization procedure. The MIP and NIP films, deposited on the colloidal crystal coated Au coated glass slides, were dipped for 5 min in 5% HF to dissolve the NPs resulting in the final macroporous MIP or NIP film.

Results and Discussion

A combined, hierarchical template for further electrosynthesis of a nanostructured MIP was prepared, as follows. First, the colloidal crystal of SiO_2 NPs (500 nm in diameter, propylamine surface-functionalized) was prepared using the Langmuir-Blodgett (LB) technique (Scheme 1 I).

The LB technique allowed depositing these NPs as four well-organized monolayers. Then, the surface of these NPs was activated with glutaraldehyde (BII in Scheme 1). Subsequently, template molecules of HSA, derivatized with bithiophene functional monomers (Cieplak et al. 2015), were immobilized on the surface of the NPs (B III in Scheme 1). This labeling assured precise controlling location of molecular cavities formed and, moreover, incurred the desired orientation of the functional monomer molecules. Finally, the empty voids between NPs of SiO_2 were filled with poly(2,3'-bithiophene) (BIV in Scheme 1). For that, we electropolymerized 2,3'-bithiophene under potentiostatic conditions.

The cross-linking monomer was selected from a group of three bithiophenes, namely 2,2'-bithiophene, 2,3'-bithiophene, and 3,3'-bithiophene. Poly(2,3'-bithiophene) was more cross-linked than the polymer resulting from electropolymerization of 2,2'-bithiophene. Hence, the structure of imprinted molecular cavities was more rigid and stable. On the other hand, oxidation potential of 2,3'-bithiophene (~1.00 V vs. Ag|AgCl pseudo- reference electrode) is, advantageously, much lower than that of 3,3'-bithiophene (~1.40 V vs. Ag|AgCl pseudo-reference electrode).

Preliminary surface immobilization of functional monomer-coupled HSA enabled subsequent poly(2,3'-bithiophene) depositing from propylene carbonate (PC), a solvent in which HSA is insoluble. This solvent was used for 2,3'-bithiophene electropolymerization because of two reasons. Firstly, it is water immiscible. Therefore, PC does not extract structural water from protein molecules and, hence, the three-dimensional structure of the HSA remains intact in the course of electropolymerization. Secondly, the poly(2,3'-bithiophene) film grows from the bottom to the top of the colloidal crystal during the electropolymerization in the PC.

[Here Figure 1]

This growth was for the first time optimized to such an extent that it was possible to observe slight current oscillations during potentiostatic deposition of poly(2,3'-bithiophene) within the colloidal crystal (Figure 1b and 1c). Noticeably, functional monomers located on the HSA surface are co-polymerized with poly(2,3'-bithiophene) matrix during this process, thus constituting a part of the polymer. The voids between NPs of SiO_2 were completely filled with poly(2,3'-thiophene), apparently resulting in an inverse opal polymer structure (Figure 2c-2f).

Both high mechanical and chemical stability of poly(2,3'-bithiophene) enabled dissolving the SiO_2 colloidal crystal with hydrofluoric acid, followed by release of the HSA template via hydrolysis under strong basic conditions. This two-step removal procedure resulted in formation of a semi-covalently surface-imprinted poly(2,3'-bithiophene) inverse opal film with functional groups embedded in the molecular cavities. XPS spectra indicated a pronounced drop of N 1s signal when the immobilized protein molecules were coated with the poly(2,3'-thiophene) film (Figure S2 IV). This is because ~2.5 layers of SiO_2 NPs colloidal crystal were coated with polythiophene film. Therefore, HSA molecules immobilized on the top uncoated 1.5 layer were still exposed on the surface. After subsequent colloidal crystal and protein template removal, the relative content of nitrogen significantly decreased (Figure S2 V). The N 1s signal observed in this step originated from the nitrogen containing functional monomer which amine moieties were located directly on the surface of molecular cavities. The 3-D hierarchical structure of the deposited nanomaterial is constructed of interconnected macropores (Figure 2 c-f) with nanocavities imprinted with HSA molecules on the internal surface of the macropores. The calculated specific surface area of the inverse opals polymer film composed of 2.5 layers of spherical pores is 8.88 times higher compared to a continuous polymer film of the same projected area. Moreover, the rather large size of the spherical pores and interconnections between them ensured easy permeation of the HSA analyte molecules to the cavities, thus resulting in high sensitivity, detectability, and fast response of a chemosensor using this film as recognition material. Semi-covalent HSA imprinting leads to location of all functional monomer moieties on the surface of molecular cavities (Cieplak et al. 2015). These moieties occupy positions complementary to those of functional groups present on the surface of the template molecule.

[Here Figure 2]

An extended-gate field-effect transistor setup (EG-FET) offers a very attractive possibility for studies of protein binding in MIP films. It combines sensitivity of FET-based sensors with ease of gate modification. The EG-FET transduction is sensitive to changes in charge concentration near the FET extended gate which influences current passing between source and drain of the transistor. Therefore, binding of charged species, e.g., proteins, in the MIP film deposited on the surface of the transistor's extended gate leads to source-drain current

change proportional to the accumulated charge. In solutions of pH far from their isoelectric points, protein molecules are highly charged where this transduction method allows highly sensitive determination of such analytes. Moreover, integration of EG-FET with an MIP recognition film (Dabrowski et al. 2016; Iskierko et al. 2016; Iskierko et al. 2015) for protein determination has not been extensively explored, so far. That way, improvement of chemosensor`s operational parameters is governed not only by advancement of the recognizing material but also by application of an efficient and sensitive platform of signal transduction.

The electrical circuit of the system used for measurements with the (EG-FET)-MIP chemosensor is shown in the inset of Figure 3A. The HSA-MIP-coated electrode was immersed in the cell containing the test solution and connected to the commercial FET as an extended gate. Then source, drain and an extended gate of FET were connected to the two-channel source meter. A voltage of 3.00 V was subsequently applied to the gate through reference electrode also immersed in the test solution. Then, the source-drain current of the transistor was measured at a potential where current saturation was observed. In such a setup even small perturbations of potential of the MIP-coated extended gate caused by binding of charged protein in the MIP film results in a pronounced change of the source-drain current. Therefore, this method is suitable to study processes of adsorption of a charged species on the electrode surface.

[Here Figure 3]

The HSA-extracted MIP macroporous film-coated electrode was very sensitive to the HSA analyte, reaching a sensitivity of 118 μA/μM. In EG-FET determinations, the signal responded linearly to the logarithm of HSA concentration in solution in the range from 15 to 150 fM (curve 1 in Figure 3A) obeying the linear regression equation of $\Delta I\,[\mu A] = 1.974 \times 10^{-5}\ (\pm 2.9 \times 10^{-5}) \times \log(c_{HSA}, M) + 2.748 \times 10^{-4}\ (\pm 3.9 \times 10^{-6})\ [\mu A]$ with a correlation coefficient of $R^2 = 0.996$. At a HSA concentration above 1 pM no changes in source-drain current were observed. This was because all cavities of the MIP film were saturated or transistors gate became fully open. Importantly, a dynamic linear response range is far below concentrations of HSA spotted in body fluids (Figure 3B). Therefore, it is possible to perform measurements of such samples as blod serum, urine or cerebrospinal fluid. The NIP macroporous film-coated electrode was not responding to changes of the HSA concentration (curve 4 in Figure 3A) indicating

practically no non-specific binding of the protein to the film surface. Moreover, the durability of the devised chemosensor was determined. Even after two weeks of everyday measurements, sensitivity of MIP-HSA EG-FET chemosensor was not changed, only the standard deviation of measurements increased (Figure S3).

One of the most important features of each chemosensor is its high sensitivity, detectability and, what is even more important, high selectivity with respect to analyte analogues. We show here that a geometrical match ensured by semi-covalent imprinting resulted in high affinity of HSA analyte to the molecular cavities, manifested by high sensitivity, superior detectability and a very high selectivity (Figure 3). The latter aspect is illustrated by the chemosensor response to the myoglobin and cytochrome c interferences, which was indistinguishable from the noise (curves 2 and 3 in Figure 3A and Figure S3) indicating that those proteins were not binding effectively in the MIP film. Even if a molecule of an interfering protein entered the molecular cavity, the pattern of noncovalent interactions is not complementary to its structure, thus, this binding is much weaker compared to the one of HSA.

Conclusions

Application of a colloidal crystal as a solid support for derivatized protein template immobilization resulted in a combined, hierarchical nanotemplate fabrication that ensured control over preparation of a highly porous hierarchical imprinted polymer film on three lengh scale levels. Enhanced surface area of this MIP together with precise control of the imprinting cavities provided both easy access for the target protein analyte to the imprinted cavities and its selective binding. Combination of this deposited recognition layer with the sensitive EG-FET transduction allowed determination of HSA in femtomolar concentration range. This range is much lower than the HSA concentration in blood serum (530 to 750 μM) (Greipp et al. 2005), urine (<0.45 μM) (Hoogenberg et al. 1993), and cerebrospinal fluid (3 μM) (Stanyon and Viles 2012). Abnormal HSA concentration in blood serum may be correlated with coronary heart disease (Danesh et al. 1998), multiple myeloma (Greipp et al. 2005), and chronic hepatitis (Murch et al. 1996). Moreover, albuminuria is caused by kidney damage, most often resulting from diabetes and hypertension (Hoogenberg et al. 1993). Threfore, developing a chemosensor for selective HSA determination is important for clinical diagnostics. The present research brings

significant improvement with respect to the performance of previously reported MIP chemosensors for HSA (Cieplak et al. 2015; Inoue et al. 2013; Lin et al. 2004; Zhang et al. 2006). The presented high detectability, due to a synergy of the macroporous structuring of the MIP film and surface semi-covalent imprinting, is one of the highest reported for all MIP chemosensors ever (Cai et al. 2010; Li et al. 2015; Li et al. 2013; Silva et al. 2016; Wang et al. 2013). Moreover, the precise geometrical fit of the imprinted cavities to the HSA molecules ensured by a semi-covalent approach resulted in a very high selectivity of the deposited MIP film. The fabricated MIP-HSA chemosensor responded neither to myoglobin nor to cytochrome *c* interfering proteins. Flexibility is one the greatest advantages of the procedure developed herein. A similar procedure can easily be extended to the fabrication of MIP based chemosensors for selective determination of other proteins and, in general, to other challenging macromolecular analytes.

Acknowledgements

The authors acknowledge the National Science Center of Poland (Grant No. NCN 2014/15/B/ST4/04642 to K.N.) and European Regional Development Fund through Project ERDF (POIG.01.01.02-00-008/08 2007-2013 to W.K., M.D., K.N., P.S.S.) for financial support.

References

Bartlett, P.N., Birkin, P.R., Ghanem, M.A., Toh, C.-S., 2001. Electrochemical syntheses of highly ordered macroporous conducting polymers grown around self-assembled colloidal templates. J. Mater. Chem. 11, 849-853.

Bognar, J., Szucs, J., Dorko, Z., Horvath, V., Gyurcsanyi, R.E., 2013. Nanosphere lithography as a vrsatile mthod to gnerate srface-iprinted plymer flms for slective potein rcognition. Adv. Funct. Mater. 23, 4703-4709.

Bompart, M., Haupt, K., Ayela, C., 2012. Micro and nanofabrication of molecularly imprinted polymers. Top. Curr. Chem. 325, 83-110.

Bossi, A., Bonini, F., Turner, A.P.F., Piletsky, S.A., 2007. Molecularly imprinted polymers for the recognition of proteins: The state of the art. Biosens. Bioelectron. 22, 1131-1137.

Cai, D., Ren, L., Zhao, H.Z., Xu, C.J., Zhang, L., Yu, Y., Wang, H.Z., Lan, Y.C., Roberts, M.F., Chuang, J.H., Naughton, M.J., Ren, Z.F., Chiles, T.C., 2010. A molecular-imprint nanosensor for ultrasensitive detection of proteins. Nat. Nanotechnol. 5, 597-601.

Cassagneau, T., Caruso, F., 2002. Semiconducting Polymer Inverse Opals Prepared by Electropolymerization. Adv. Mater. 14, 34-38.

Choi, G.H., Rhee, D.K., Park, A.R., Oh, M.J., Hong, S., Richardson, J.J., Guo, J.L., Caruso, F., Yoo, P.J., 2016. Ag nanoparticle/polydopamine-coated inverse opals as highly efficient catalytic membranes. ACS Appl. Mater. Inter. 8, 3250-3257.

Cieplak, M., Szwabinska, K., Sosnowska, M., Bikram, K.C.C., Borowicz, P., Noworyta, K., D'Souza, F., Kutner, W., 2015. Selective electrochemical sensing of human serum albumin by semi-covalent molecular imprinting. Biosens. Bioelectron. 74, 960-966.

Collins, G., Blomker, M., Osiak, M., Holmes, J.D., Bredol, M., O'Dwyer, C., 2013. Three-dimensionally ordered hierarchically porous tin dioxide inverse opals and immobilization of palladium nanoparticles for catalytic applications. Chem. Mater. 25, 4312-4320.

Dabrowski, M., Sharma, P.S., Iskierko, Z., Noworyta, K., Cieplak, M., Lisowski, W., Oborska, S., Kuhn, A., Kutner, W., 2016. Early diagnosis of fungal infections using piezomicrogravimetric and electric chemosensors based on polymers molecularly imprinted with D-arabitol. Biosens. Bioelectron. 79, 627-635.

Danesh, J., Collins, R., Appleby, P., Peto, R., 1998. Association of fibrinogen, C-reactive protein, albumin, or leukocyte count with coronary heart disease - Meta-analyses of prospective studies. Jama-J. Am. Med. Assoc. 279, 1477-1482.

Dechtrirat, D., Jetzschmann, K.J., Stocklein, W.F.M., Scheller, F.W., Gajovic-Eichelmann, N., 2012. Protein rebinding to a surface-confined imprint. Adv. Funct. Mater. 22, 5231-5237.

Diao, Y.Y., Liu, X.Y., Toh, G.W., Shi, L., Zi, J., 2013. Multiple structural coloring of silk-fibroin photonic crystals and humidity-responsive color sensing. Adv. Funct. Mater. 23, 5373-5380.

Duffel, B.v., Ras, R.H.A., Schryver, F.C.D., Schoonheydt, R.A., 2001. Langmuir–Blodgett deposition and optical diffraction of two-dimensional opal. J. Mater. Chem., 3333-3336.

Erdossy, J., Horvath, V., Yarman, A., Scheller, F.W., Gyurcsanyi, R.E., 2016. Electrosynthesized molecularly imprinted polymers for protein recognition. TrAC-Trend. Anal. Chem. 79, 179-190.

Greipp, P.R., San Miguel, J., Durie, B.G.M., Crowley, J.J., Barlogie, B., Blade, J., Boccadoro, M., Child, J.A., Harousseau, J.L., Kyle, R.A., Lahuerta, J.J., Ludwig, H., Morgan, G., Powles, R., Shimizu, K., Shustik, C., Sonneveld, P., Tosi, P., Turesson, I., Westin, J., 2005. International staging system for multiple myeloma. J Clin Oncol 23, 3412-3420.

Heim, M., Reculusa, S., Ravaine, S., Kuhn, A., 2012. Engineering of Complex Macroporous Materials Through Controlled Electrodeposition in Colloidal Superstructures. Adv. Funct. Mater. 22, 538-545.

Holtz, J.H., Holtz, J.S.W., Munro, C.H., Asher, S.A., 1998. Intelligent Polymerized Crystalline Colloidal Arrays: Novel Chemical Sensor Materials. Anal. Chem. 70, 780-791.

Hoogenberg, K., Sluiter, W.J., Dullaart, R.P., 1993. Effect of growth hormone and insulin-like growth factor I on urinary albumin excretion: studies in acromegaly and growth hormone deficiency. Acta endocrinologica 129, 151-157.

Hu, X.B., Li, G.T., Huang, J., Zhang, D., Qiu, Y., 2007. Construction of self-reporting specific chemical sensors with high sensitivity. Adv. Mater. 19, 4327-4332.

Hu, X.B., Li, G.T., Li, M.H., Huang, J., Li, Y., Gao, Y.B., Zhang, Y.H., 2008. Ultrasensitive specific stimulant assay based on molecularly imprinted photonic hydrogels. Adv. Funct. Mater. 18, 575-583.

Huynh, T.-P., Sharma, P.S., Sosnowska, M., D'Souza, F., Kutner, W., 2015. Functionalized polythiophenes: Recognition materials for chemosensors and biosensors of superior sensitivity, selectivity, and detectability. Prog. Polym. Sci. 47, 1-25.

Inoue, Y., Kuwahara, A., Ohmori, K., Sunayama, H., Ooya, T., Takeuchi, T., 2013. Fluorescent molecularly imprinted polymer thin films for specific protein detection prepared with dansyl ethylenediamine-conjugated *O*-acryloyl L-hydroxyproline. Biosens. Bioelectron. 48, 113-119.

Iskierko, Z., Sharma, P.S., Prochowicz, D., Fronc, K., D'Souza, F., Toczydlowska, D., Stefaniak, F., Noworyta, K., 2016. Molecularly imprinted polymer (MIP) film with improved surface area developed by using metal-organic framework (MOF) for sensitive lipocalin (NGAL) determination. ACS Appl. Mater. Inter. 8, 19860-19865.

Iskierko, Z., Sosnowska, M., Sharma, P.S., Benincori, T., D'Souza, F., Kaminska, I., Fronc, K., Noworyta, K., 2015. Extended-gate field-effect transistor (EG-FET) with molecularly imprinted polymer (MIP) film for selective inosine determination. Biosens. Bioelectron. 74, 526-533.

Kuo, C.-Y., Lu, S.-Y., Chen, S., Bernards, M., Jiang, S., 2007. Stop band shift based chemical sensing with three-dimensional opal and inverse opal structures. Sen. Actuators, B 124, 452-458.

Lautner, G., Kaev, J., Reut, J., Opik, A., Rappich, J., Syritski, V., Gyurcsanyi, R.E., 2011. Selective artificial receptors based on micropatterned surface-imprinted polymers for label-free detection of proteins by SPR imaging. Adv. Funct. Mater. 21, 591-597.

Li, L., Fan, L.M., Dai, Y.L., Kan, X.W., 2015. Recognition and determination of bovine hemoglobin using a gold electrode modified with gold nanoparticles and molecularly imprinted self-polymerized dopamine. Microchim. Acta 182, 2477-2483.

Li, L., Yang, L.L., Xing, Z.L., Lu, X.J., Kan, X.W., 2013. Surface molecularly imprinted polymers-based electrochemical sensor for bovine hemoglobin recognition. Analyst 138, 6962-6968.

Li, S.J., Cao, S.S., Whitcombe, M.J., Piletsky, S.A., 2014. Size matters: Challenges in imprinting macromolecules. Prog. Polym. Sci. 39, 145-163.

Li, X.H., Dai, L., Liu, Y., Chen, X.J., Yan, W., Jiang, L.P., Zhu, J.J., 2009. Ionic-liquid-doped polyaniline inverse opals: preparation, characterization, and application for the electrochemical impedance immunoassay of Hepatitis B surface antigen. Adv. Funct. Mater. 19, 3120-3128.

Li, Y., Fu, Z.Y., Su, B.L., 2012. Hierarchically structured porous materials for energy conversion and storage. Adv. Funct. Mater. 22, 4634-4667.

Lin, T.Y., Hu, C.H., Chou, T.C., 2004. Determination of albumin concentration by MIP-QCM sensor. Biosens. Bioelectron. 20, 75-81.

Linares, A.V., Vandevelde, F., Pantigny, J., Falcimaigne-Cordin, A., Haupt, K., 2009. Polymer films composed of surface-bound nanofilaments with a high aspect ratio, molecularly imprinted with small molecules and proteins. Adv. Funct. Mater. 19, 1299-1303.

Liu, S., Zhou, D.Z., Guo, T.Y., 2013. Construction of a novel macroporous imprinted biosensor based on quartz crystal microbalance for ribonuclease A detection. Biosens. Bioelectron. 42, 80-86.

Murch, S.H., Winyard, P.J., Koletzko, S., Wehner, B., Cheema, H.A., Risdon, R.A., Phillips, A.D., Meadows, N., Klein, N.J., Walker-Smith, J.A., 1996. Congenital enterocyte heparan sulphate deficiency with massive albumin loss, secretory diarrhoea, and malnutrition. Lancet 347, 1299-1301.

Reculusa, S., Heim, M., Gao, F., Mano, N., Ravaine, S., Kuhn, A., 2011. Design of Catalytically Active Cylindrical and Macroporous Gold Microelectrodes. Adv. Funct. Mater. 21, 691-698.

Reculusa, S., Massé, P., Ravaine, S., 2004. Three-dimensional colloidal crystals with a well-defined architecture. J. Colloid Interface Sci. 279, 471-478.

Reculusa, S., Ravaine, S., 2003. Synthesis of colloidal crystals of controllable thickness through the Langmuir-Blodgett technique. Chem. Mater. 15, 598-605.

Reculusa, S., Ravaine, S., 2005. Colloidal photonic crystals obtained by the Langmuir–Blodgett technique. Appl. Surf. Sci. 246, 409-414.

Silva, B.V.M., Rodriguez, B.A.G., Sales, G.F., Sotomayor, M.D.T., Dutra, R.F., 2016. An ultrasensitive human cardiac troponin T graphene screen-printed electrode based on electropolymerized-molecularly imprinted conducting polymer. Biosens. Bioelectron. 77, 978-985.

Stanyon, H.F., Viles, J.H., 2012. Human serum albumin can regulate amyloid-beta peptide fiber growth in the brain interstitium implications for Alzheimer Disease. J Biol Chem 287, 28163-28168.

Szamocki, R., Reculusa, S., Ravaine, S., Bartlett, P.N., Kuhn, A., Hempelmann, R., 2006. Tailored Mesostructuring and Biofunctionalization of Gold for Increased Electroactivity. Angew. Chem. Internt. Ed. 45, 1317-1321.

Szucs, J., Lindfors, T., Bobacka, J., Gyurcsanyi, R.E., 2016. Ion-selective electrodes with 3D nanostructured conducting polymer solid contact. Electroanal. 28, 778-786.

Walcarius, A., 2010. Template-directed porous electrodes in electroanalysis. Anal. Bioanal. Chem. 396, 261-272.

Wang, X., Husson, S.M., Qian, X., Wickramasinghe, S.R., 2010. Inverse colloidal crystal microfiltration membranes. J. Membr. Sci. 365, 302-310.

Wang, X.D., Dong, J., Ming, H.M., Ai, S.Y., 2013. Sensing of glycoprotein via a biomimetic sensor based on molecularly imprinted polymers and graphene-Au nanoparticles. Analyst 138, 1219-1225.

Yang, Z.J., Xie, Z.Y., Liu, H., Yan, F., Ju, H.X., 2008. Streptavidin-functionalized three-dimensional ordered nanoporous silica film for highly efficient chemiluminescent immunosensing. Adv. Funct. Mater. 18, 3991-3998.

Zdunek, J., Benito-Pena, E., Linares, A., Falcimaigne-Cordin, A., Orellana, G., Haupt, K., Moreno-Bondi, M.C., 2013. Surface-imprinted nanofilaments for europium-amplified luminescent dtection of fuoroquinolone atibiotics. Chem.-Eur. J. 19, 10209-10216.

Zhang, Z., Long, Y., Nie, L., Yao, S., 2006. Molecularly imprinted thin film self-assembled on piezoelectric quartz crystal surface by the sol-gel process for protein recognition. Biosens. Bioelectron. 21, 1244-1251.

Zhao, L., Tong, L., Li, C., Gu, Z., Shi, G., 2009. Polypyrrole actuators with inverse opal structures. J. Mater. Chem. 19, 1653-1658.

Zheng, H.B., Vallee, R., Almeida, R.M., Rivera, T., Ravaine, S., 2014. Quasi-omnidirectional total light absorption in nanostructured gold surfaces. Opt. Mater. Express 4, 1236-1242.

Zhou, D.Z., Guo, T.Y., Yang, Y., Zhang, Z.P., 2011. Surface imprinted macroporous film for high performance protein recognition in combination with quartz crystal microbalance. Sens. Actuators, B 153, 96-102.

Scheme 1. (A 1) 3-D structure of HSA (http://www.rcsb.org/pdb/explore/explore.do?pdbId=1E7H), structural formulas of (A 2) functional monomers and (A 3) the cross-linking monomer. (B) Illustration of the elaboration procedure of the poly(2,3'-bithiophene) inverse opal imprinting with HSA.

Figure 1. Changes of current with time during potentiostatic deposition of (*1*) NIP on a bare Au-coated glass slide as well as (*2*) the molecularly imprinted polymer (MIP) and (*3*) non-imprinted polymer (NIP) on the Au-coated glass slide with the deposited four-layer 500-nm NP colloidal crystal. The propylene carbonate solution used was 0.5 M in the 2,3'-bithiophene cross-linking monomer and 3.0 M in the $LiClO_4$ supporting electrolyte. The potential was hold at 1.30 V vs. Ag|AgCl pseudo-reference electrode.

Figure 2. The (a, c, and e) side and (b, d, and f) top views of SEM images of (a and b) a colloidal crystal consisting of four-layers of 500-nm diameter silica NPs, (c and d) the HSA template extracted MIP-HSA film, and (e and f) the macroporous NIP film deposited on Au electrodes.

Figure 3. (A) Calibration plots for the EG-FET chemosensor with its gate coated with the macroporous MIP-HSA film for (1) HSA as well as its interferences (2) myoglobin and (3) cytochrome c as well as (4) for the EG-FET chemosensor with its gate coated with the macroporous NIP film. Inset shows experimental setup based on the EG-FET design using the Au-glass slide, coated with an MIP-HSA or NIP film, and a Pt plate as the gate (working electrode, WE) and the reference electrode (RE), respectively. G, D, and S stand for the gate, drain, and source components of the FET structure, respectively. The reference electrode was polarized to the gate voltage, V_R = 3.00 V. (B) Detectability and linear dynamic concentration range of the EG-FET chemosensor with the macroporous MIP-HSA film in comparison to HSA concentration in body fluids.

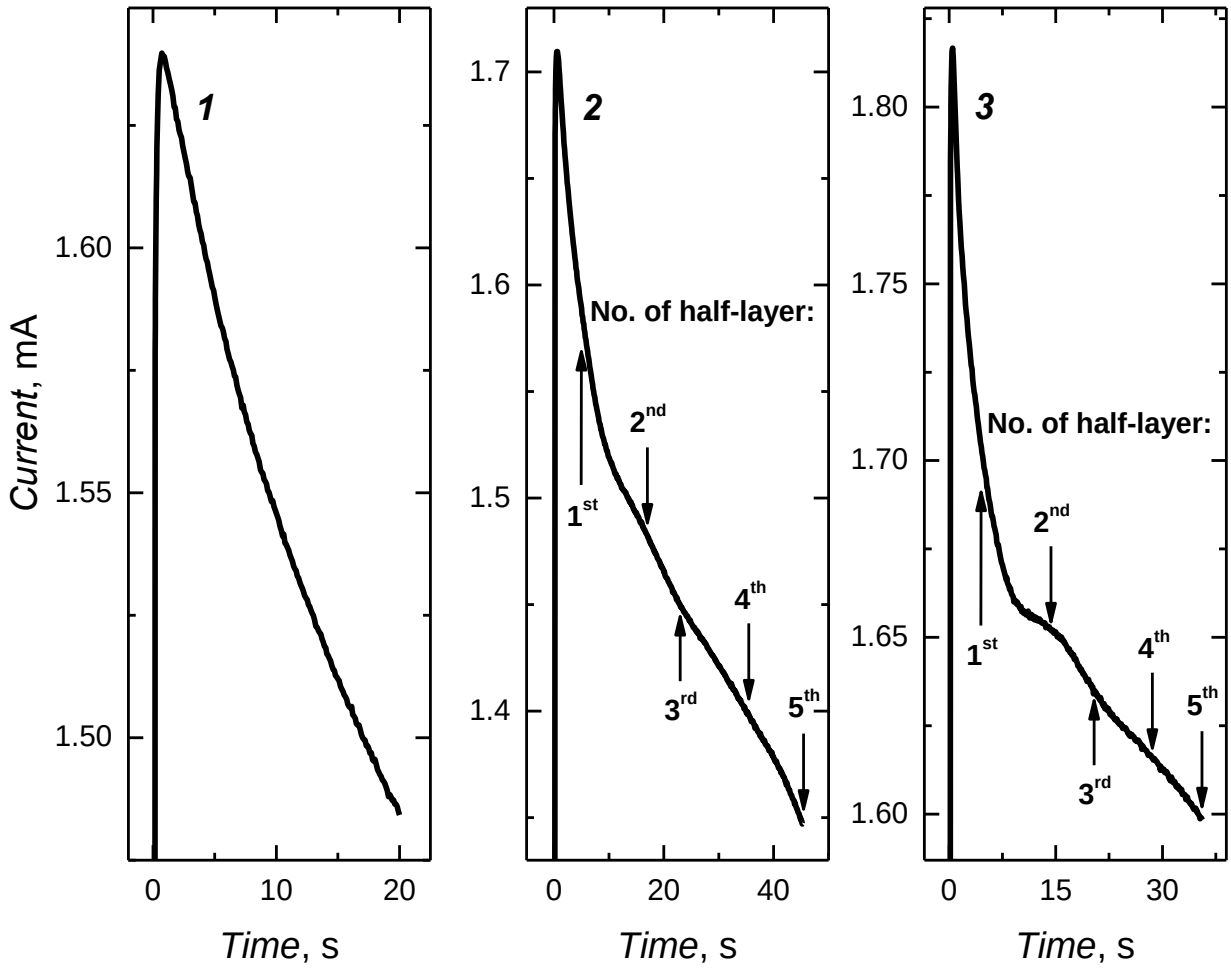

Figure 1

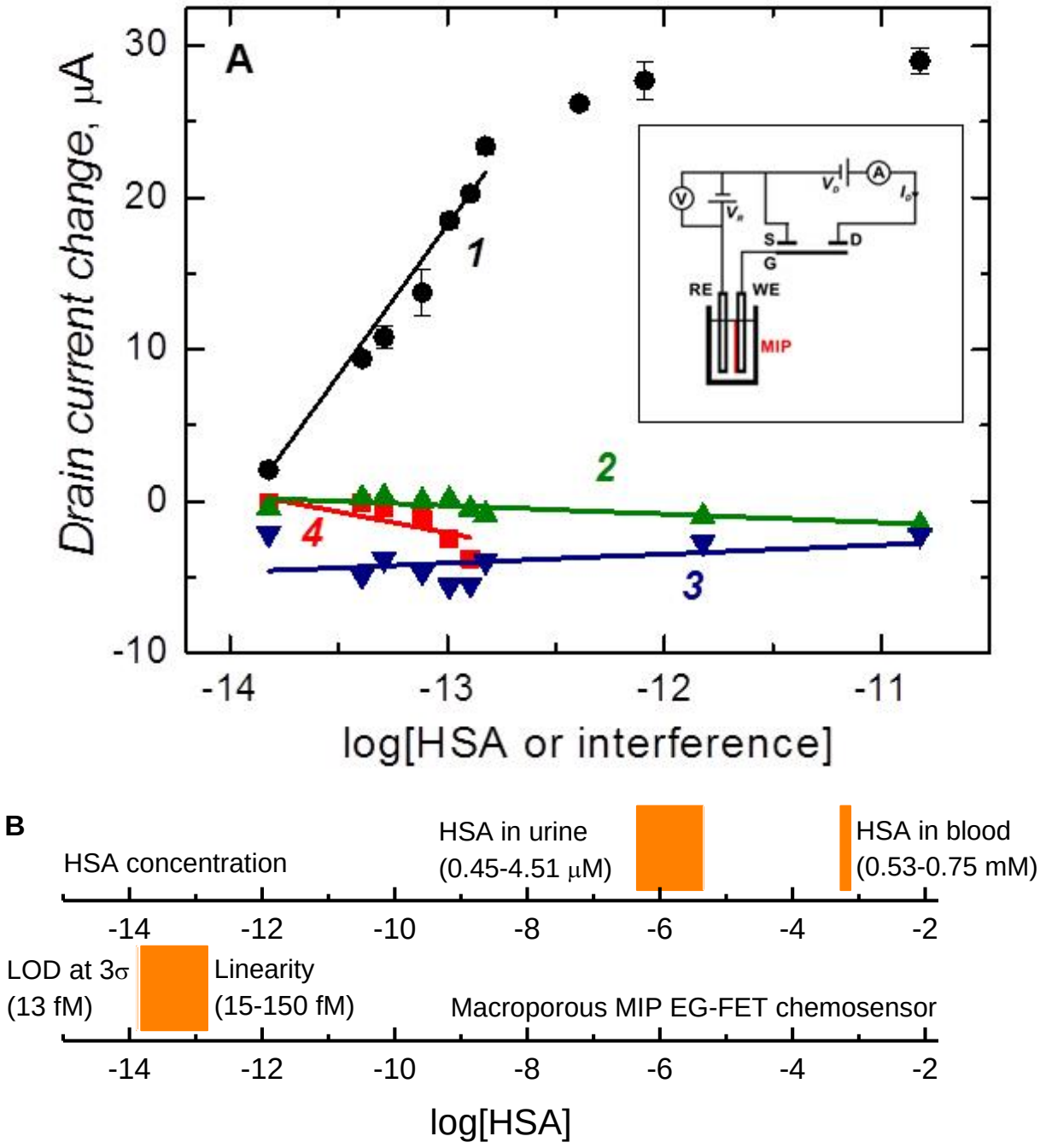

Figure 3